Developmental Cell, Vol. 8, 215–227, February, 2005, Copyright ©2005 by Elsevier Inc. DOI 10.1016/j.devcel.2004.12.007

A Local Coupling Model and Compass Parameter for Eukaryotic Chemotaxis

Cécile Arrieumerlou and Tobias Meyer*
Department of Molecular Pharmacology
Stanford University School of Medicine
Stanford, California 94305

Summary

Chemotaxis is a cellular sensing mechanism that guides immune cells to sites of infection and leads fibroblasts to sites of injury. Here, we show in migrating primary dendritic cells and fibroblasts that the leading edge is not a uniform signaling entity, but instead consists of independent coupling units in which transient activation of PI3-kinase links to local lamellipod extension and small discrete turns in the direction of migration. These findings led to a model in which global cell polarization is independent from the chemotaxis mechanism. In this model, chemotaxis does not require spatial integration but is instead a stochastic process in which each receptor binding event within the leading edge triggers a local lamellipod extension and a small turn in the direction of migration. We show that this model and a derived "compass parameter" are sufficient to simulate the observed random migration, biased random walk, and persistent chemotactic behaviors of eukaryotic cells.

Introduction

Chemotaxis is a ubiquitous cellular process that enables budding yeast to find mating partners and amoebae such as *Dictyostelium discoideum* to form a multicellular organism (Parent and Devreotes, 1999; Schrick et al., 1997). In higher eukaryotes, chemotaxis enables differentiated cells to move to their target location or crawl to sites of infection and tissue injury (Downey, 1994). Chemotaxing eukaryotic cells are all commonly highly polarized and contain actin-based cytoskeletal components, membrane lipids, and signaling proteins that are asymmetrically distributed between the front and the back of the migrating cell (Funamoto et al., 2002; Iijima and Devreotes, 2002; Postma et al., 2004; Zigmond et al., 1981). The enriched actin-polymerization machinery at the leading edge supports extensions of lamellipods in the direction of migration (Condeelis et al., 1988; Pollard and Borisy, 2003; Schmidt and Hall, 1998). This extension allows newly created adhesions within the extended membranes to then function as traction sites that allow cells to move forward.

Frequently discussed quantitative models for chemotaxis (Kutscher et al., 2004; Levchenko and Iglesias, 2002; Meinhardt, 1999) are based on "gradient amplification" and propose that small gradients in chemoattractant are amplified in cells so that the externally applied chemoattractant gradient is translated into an internal cell polarity with 3′ phosphoinositide lipids (PI3Ps) and lamellipod extension that is oriented toward the source of the chemoattractant (Funamoto et al., 2002; Haugh et al., 2000; Iijima and Devreotes, 2002; Janetopoulos et al., 2004; Meili et al., 1999; Parent et al., 1998; Servant et al., 2000; Hannigan et al., 2002; Niggli, 2000). Several of these models are based on positive feedback triggered at the site closest to the source combined with cell-wide negative feedback (Xu et al., 2003; Postma et al., 2004).

These models as well as an earlier fluctuation model (Tranquillo et al., 1988) have in common that they assume a spatial cell-wide integration of individual receptor stimuli that defines a direction of the chemoattractant source. Nevertheless, they have not addressed why and how cells in shallow gradients undergo a biased random walk toward such a source, why and how they can make smooth turns if they encounter a new directional signal, or why or how they undergo random migration in uniform chemoattractant.

Here, we propose that chemotaxis is a process that occurs on top of a more basic process of selfpolarization and show evidence that spatial sensing is a result of local coupling of a receptor stimulus to a local lamellipod extension within an established leading edge of a polarized and migrating cell. Thus, instead of postulating that spatial signal integration contributes to chemotaxis, this model separates a global selfpolarization process from a local chemotaxis process that operates in already polarized cells. In the proposed "local coupling model" for eukaryotic chemotaxis, each receptor stimulus within the leading edge is coupled to a unitary local lamellipod extension that leads to a small turn to the left if the local extension is on the left and to the right if the local extension is on the right. This model assumes that there are independent spatial signaling domains within the leading edge that are each capable of triggering local lamellipod extension. Statistically, the assumption of local coupling more often creates direction changes toward the chemoattractant source than away from it, and we show that this is sufficient to simulate the observed migration behavior. We further found that the resulting stochastic migration behavior can be predicted by a simple chemotaxis equation and "compass parameter" that describes the directional choices of cells and explains how they randomly migrate, how they undergo random biased walks, or how they undergo persistent chemotaxis.

Our model was derived by tracking cells during migration and chemotaxis, by measuring local lamellipod extension processes that occur within the leading edge of migrating cells, by monitoring local pulses of PI3-kinase (PI3K) activation, and by simulation and quantitative modeling of the chemotaxis process. In order to ensure that we were not investigating a cell-specific phenomenon, we chose two distinct model systems for cell migration: primary DCs and C5a as a G protein-coupled chemoattractant and fibroblasts and platelet-

*Correspondence: Tobiasmeyer@stanford.edu

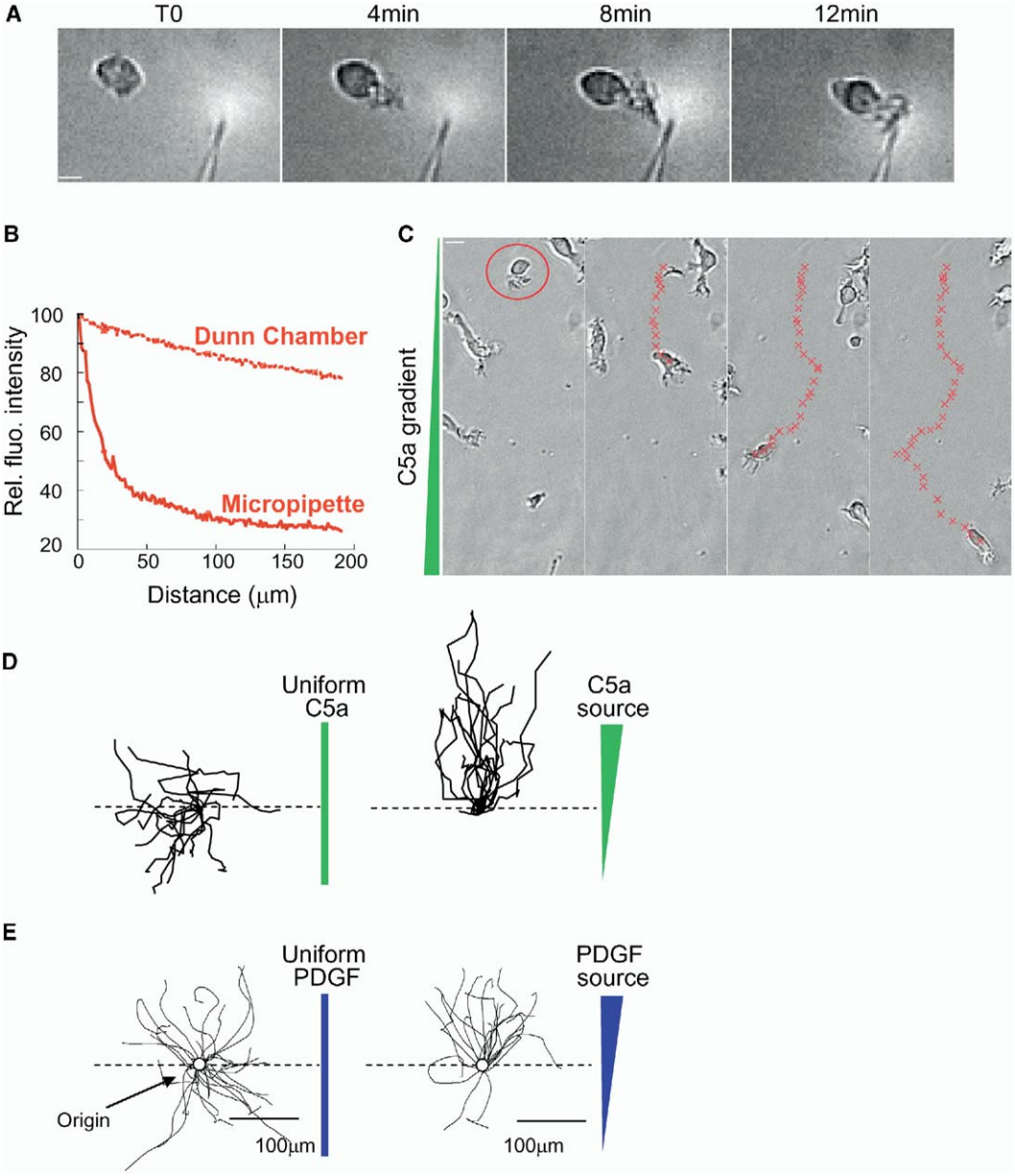

Figure 1. Cell Migration in Decreasing Chemoattractant Gradients: Persistent Chemotaxis, Biased Random Migration, and Random Migration of DCs and Fibroblasts

(A) Persistent migration of a DC toward a micropipette filled with C5a (0.45 μM). Scale bar, 10 μm.
(B) Comparison of relative rhodamine dextran gradient profiles generated by a micropipette and in a Dunn chamber.
(C) Example of biased random walk of a DC in response to a shallow C5a gradient (45 nM; 2%–4% across a cell). Scale bar, 10 μm.
(D and E) Experimental migration traces (over 120 min) obtained in a Dunn chamber in uniform chemoattractant and in the presence of a shallow chemoattractant gradient. DCs in C5a are shown in (D), and fibroblasts in PDGF are shown in (E).

derived growth factor (PDGF) as a tyrosine kinase-coupled chemoattractant.

Results and Discussion

Characterization of Cell Migration in Steep, Shallow, and Uniform Concentration Gradients

Since primary human DCs have not yet been visualized during chemotaxis, we monitored their migration in the presence of a gradient of C5a, an important chemoattractant that guides DCs to sites of infection (Mrowietz et al., 2001; Sozzani et al., 1995). Similar to previous studies in *Dictyostelium discoideum* and in an HL-60 neutrophil cell line, the chemoattractant was presented focally by placing a micropipette loaded with C5a near to the cell to create a chemoattractant gradient (Figures 1A and 1B). Consistent with previous findings, unpolarized DCs became polarized and migrated

toward the pipette (Figure 1A; example out of nine experiments; see Supplemental Movie S1 in the Supplemental Data available with this article online) (Bailly et al., 2000; Servant et al., 1999). DCs that were already polarized could also be made to redirect their migration by moving the micropipette to a new location, creating a migration path that was most often directed toward the direction of the pipette after an initial turn of the leading edge (data not shown; Xu et al., 2003). This ability to turn and directly migrate toward a pipette filled with chemoattractant is termed below a persistent chemotaxis process.

The concentration gradients that we created with the micropipette were initially quite steep, changed over time, and were nonlinear as the cells got closer to the pipette (Figure 1B). We therefore used a Dunn chamber to generate a more shallow and time-stable C5a gradient (Figure 1B) (Zicha et al., 1997; Zicha et al., 1991). When the migration of DCs was followed in these gradients (approximately 2%–4% concentration change across a cell; see the Experimental Procedures), we found that they migrated with a markedly different behavior than the persistent migration observed in micropipette experiments (Figure 1C; Supplemental Figure S1A; see Supplemental Movie S2 in the Supplemental Data). At a given time, many cells would migrate away from the source or perpendicular to the source, with the probability of migrating toward the source being higher than the probability of moving in the opposite direction (Figure 1D, right panel). The same type of biased random walk was observed for a neutrophil cell line in a Dunn chamber C5a gradient (Supplemental Figure S1B). This migration behavior can be termed a biased random walk since cells can move in all directions but over time move more often toward the chemoattractant source than away from it (see also Allen et al., 1998; Tranquillo et al., 1988; Wang et al., 2002).

When we applied C5a uniformly instead of in a shallow gradient, we observed a migration behavior that was at a first glance not significantly different from the one observed with the shallow gradient (Figure 1D, left panel). While the cells lacked a particular bias in their migration direction, this chemokinesis behavior (Lipton et al., 1971) was characterized by polarized lamellipod extensions at the front, with continuous smooth turns, and with similar migration velocities and turn rates.

Similar to the experiments with C5a, uniform PDGF led to a random walk, shallow PDGF gradients led to biased random walk, and both, again, showed similar velocities and turn behavior (Figure 1E). These migration processes may help fibroblasts to reach wounds and participate in the healing process (Deuel et al., 1991; Pierce et al., 1989).

Stochastic Turns in the Direction of Migration as a Result of Independent Lamellipod Extensions on the Left versus Right

DCs, neutrophils, and fibroblasts observed in the Dunn chamber or during random migration typically changed their migration direction by turning their leading edge (see, for example, Figures 1D and 1E; Supplemental Figure S1) (Xu et al., 2003). The first question that arises is whether the leading edge is a uniform entity that performs coordinated turns or whether changes in the direction of migration result from spatially confined lamellipod extension so that a local extension process on the left or right of the leading edge would preferentially lead to turns in that direction (Figure 2A). Membrane extensions were investigated by creating a series of binarized images of migrating cells by using cells transfected with CFP-CAAX (a plasma membrane marker). A difference mask of sequential binary images was used to identify the regions in which lamellipods were extended (see details in the Supplemental Data). While focally applied C5a triggered broad lamellipods to move toward the pipette (~40% concentration gradient across cell; Figure 2B), lamellipod extension during random migration was found to be local (Figure 2C). Visual inspection suggested that typical local lamellipod extensions in DCs were a few micrometers wide and were extended forward by a few micrometers over a time period of about 15–60 s (n = 28, tracked over 20–50 min). Similar local lamellipod extensions were also observed in shallow gradient migrating DCs and fibroblasts (Supplemental Figure S2).

A quantitative analysis of local lamellipod extension was made by measuring membrane extension along the cell circumference, F(x), in each image (recorded every 15 s in units of micrometers) and then by using an autocorrelation analysis of $G(x) = \Sigma F(x_0)*F(x_0 - x)$ (averaged over 540 image pairs from 8 cells; see the Experimental Procedures in the Supplemental Data). Consistent with the visual inspection, the resulting autocorrelation peak width, which corresponds to the width of individual lamellipodia, was 3.4 μm (Figure 2D; full width at half-maximum, red bar). A similar autocorrelation (peak width of 5 μm) was also found in migrating 3T3 fibroblasts (data not shown). This suggests that the dimensions of these local lamellipods are significantly smaller than the 20–30 μm total length of the leading edge in both cell types.

In order to determine whether the left and right of the leading edge extend lamellipodia independently, we compared the extensions on the left of the front of the cell with those on the right by measuring a current direction of migration (by following the center of mass) and by marking the left side and the right front of the leading edge. We defined as left and right front the perimeter regions that were within a 15°–60° angle to the left and right from the direction of migration. Figure 2E shows four snap shots of a migrating cell in which the two front regions are marked in blue (left region) and green (right region) (see the Experimental Procedures and Supplemental Movie S3 in the Supplemental Data). Interestingly, a comparison of the mean extension on the left versus the right as a function of time shows that there is no significant temporal correlation between the lamellipodia extensions on the left side and the right side of the migrating cell (Figure 2F shows a 16 min stretch of one cell as an example of the eight cells analyzed). The same analysis in several migrating fibroblasts also did not show a significant correlation between extension on the left and right front of the cell (data not shown).

Thus, the local nature of lamellipod extension within the leading edge effectively decouples the left from the right of the leading edge, and cells may, therefore, use

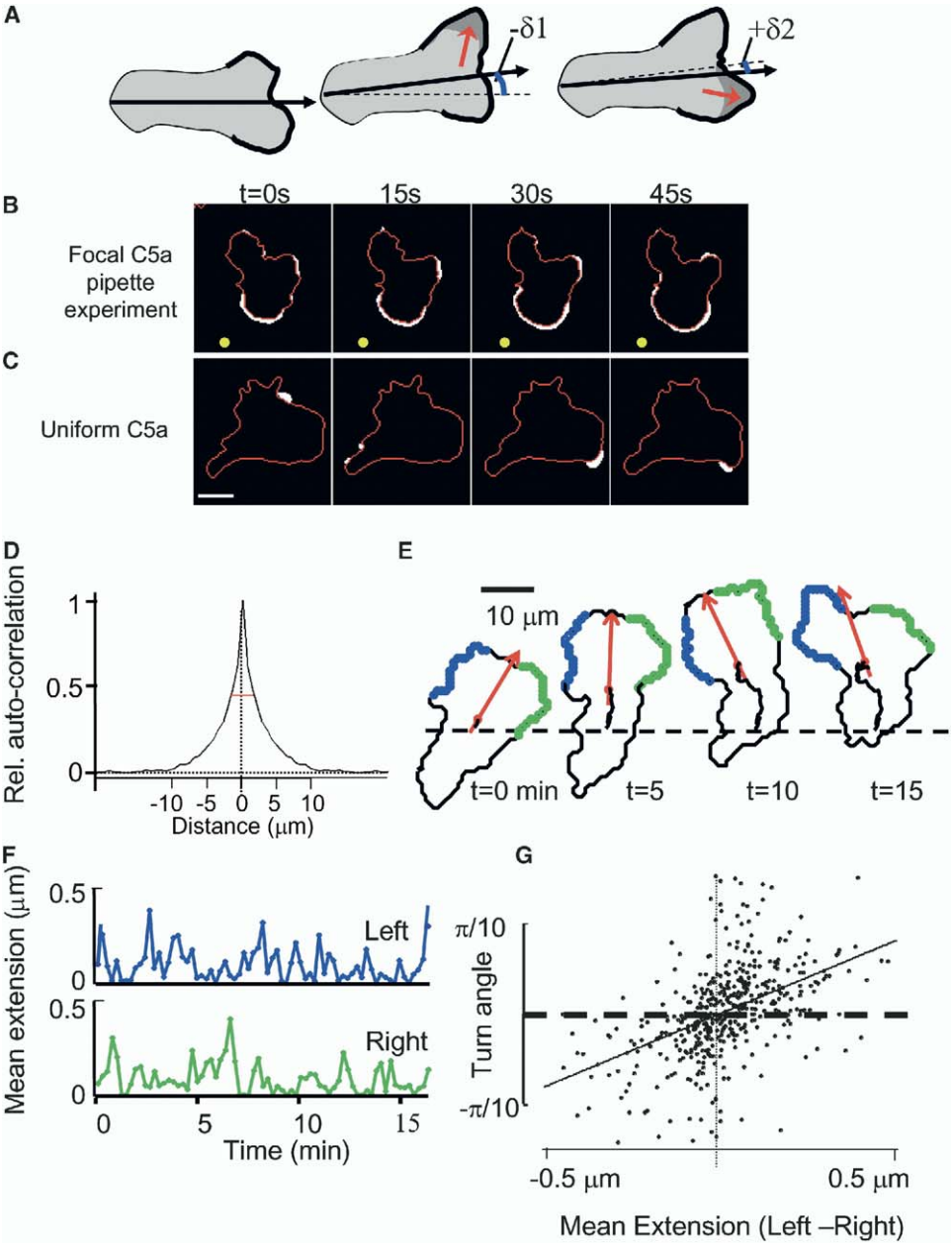

Figure 2. Stochastic Local Lamellipod Extensions within the Leading Edge Lead to Small Turns in the Direction of Migration

(A) A schematic view of how a local lamellipod may trigger a small turn to the left (angular step size $-\delta 1$) or to the right ($\delta 2$) in a migrating cell dependent on where the lamellipod extension is triggered within the leading edge.

(B) Wide membrane extensions in a DC migrating toward a C5a-filled pipette. Membrane extensions (in white) were quantified by subtraction of sequential binarized CFP-CAAX images (see the Experimental Procedures). The estimated concentration gradient is ~40%. Scale bars, 10 μm.

(C) Local membrane extensions in a DC migrating in uniform C5a.

(D) Calculation of an autocorrelation function of the local membrane extension along the cell perimeter. Lamellipodia extension was only correlated over ~3.4 μm in DCs (reflecting the mean diameter of extended lamellipods). (A correlation distance of ~5 μm was measured in fibroblasts; data not shown).

(E) Automated contour analysis and derivation of the direction of migration. The left and right regions within the leading edge are marked by the software as blue and green, respectively (see the Experimental Procedures).

(F) Time course comparison of the mean lamellipod extension (per 15 s) between the left and right side of the leading edge (marked in blue and green in Figure 2C). No significant correlation was observed, suggesting that lamellipod extension on the left and right are independent.

(G) Scatter plot representation of the differential extensions (between the left and right) versus the measured turn angle. The differential membrane extension (the mean Δ extension at the front left minus the mean Δ extension at the front right) was plotted against the turn angle. The images used to measure Δ extension and turn angle were taken 15 s apart (540 image pairs).

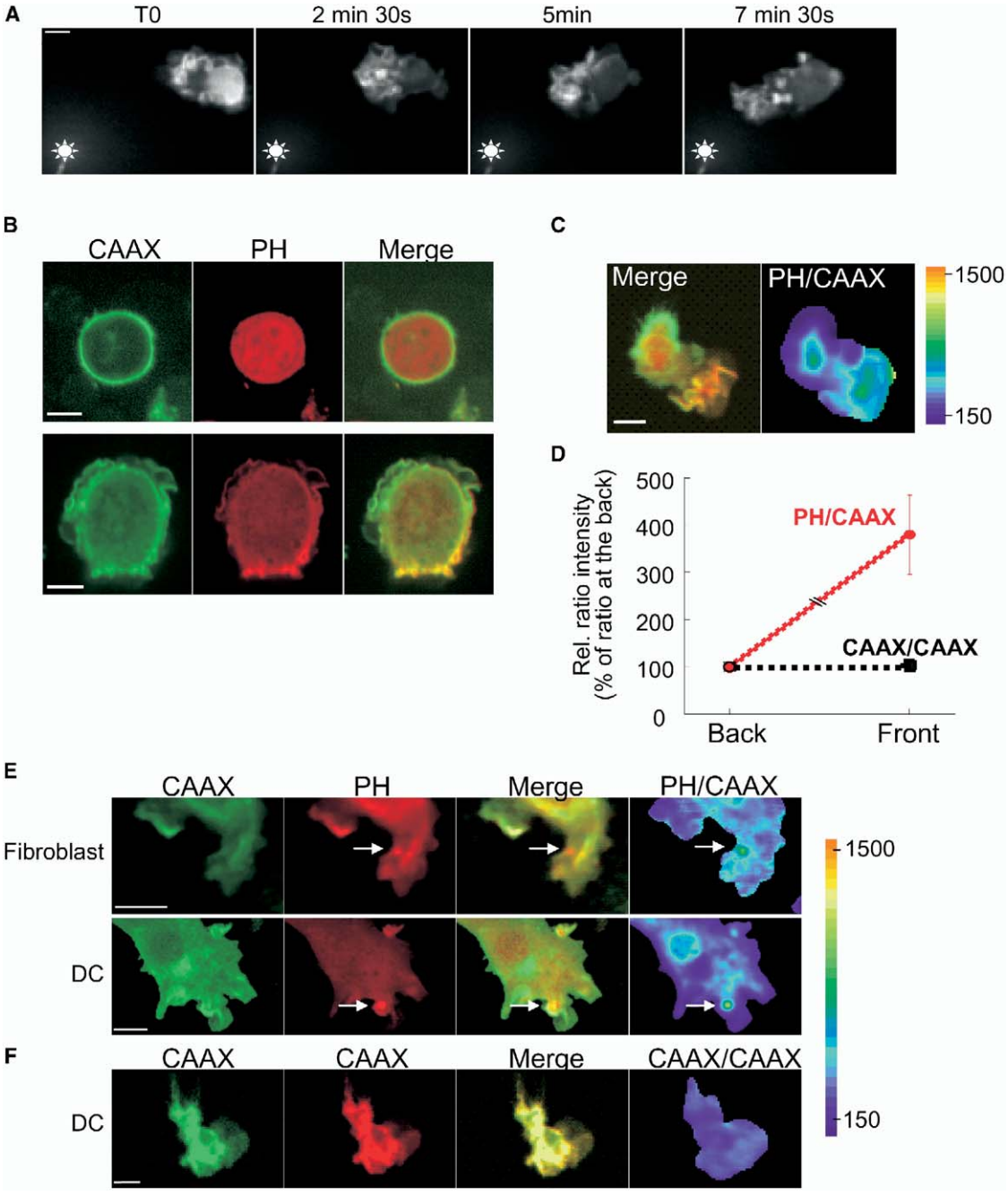

Figure 3. Front-to-Back PI3P Gradients and Local PI3P Pulses

(A) Example of PI3P accumulation at the leading edge of a DC transfected with PH(Akt)-YFP during migration toward a C5a-filled micropipette. Scale bars, 10 μm.

(B) Plasma membrane localization of a CAAX-CFP marker and membrane/cytoskeletal localization of a PH(Akt)-YFP construct in round (top panel) and in adherent (bottom panel) DCs. Midsection confocal images. Scale bars, 10 μm.

(C) Example of merged and ratio images of a DC cell showing PI3P enrichment at the leading edge. PH(Akt)-YFP and CFP-CAAX images were measured during random migration in uniform C5a concentrations. PI3P enrichment was quantified by dividing the PH(Akt)-YFP image by the CFP-CAAX image. Ratiometric analysis is shown as a pseudocolored image in the right panel.

(D) Quantification of the front-to-back PI3P gradient in DCs migrating in uniform C5a concentration. Cells cotransfected with YFP-CAAX and CFP-CAAX were used as controls (bottom line).

(E) Ratiometric measurement of PI3P pulses (white arrow) in a randomly migrating fibroblast in uniform PDGF (top panel) and in a randomly migrating DC in uniform C5a (bottom panel). Confocal images taken near the adhesion surface. All scale bars, 10 μm.

(F) Control analysis for imaging noise. Images of cells are shown cotransfected with YFP-CAAX and CFP-CAAX. Scale bar, 10 μm.

unitary local lamellipods to create stochastic small turns in the direction of migration. We tested the plausible link between asymmetric lamellipod extension at the leading edge to turns by directly plotting the turn angle as a function of the extension difference between the left and right of a cell (the mean extensions of the left leading edge region minus the mean extension of the right) (Figure 2G; 540 sequential image pairs from 8 cells). The observed correlation between asymmetric lamellipods and turns was 0.35 radian/(μm of mean extension difference) (95% confidence interval, 0.29–0.41 rad/μm), suggesting that each local lamellipod extension triggers a small turn in the direction of migration.

Two Modes of PI3K Signaling: Front-to-Back PI3P Gradients and Local Pulses of PI3P Lipid Production

A series of studies in *Dictyostelium* (Meili et al., 1999), neutrophils (Servant et al., 2000), and fibroblasts (Haugh et al., 2000) showed that PI3K signaling is polarized in cells toward a focally applied pipette containing chemoattractant. Here, we investigated PI3K signaling in primary DCs by expressing a YFP-conjugated PH domain from Akt (PH[Akt]-YFP) (Kontos et al., 1998) that binds to 3′ phosphorylated PI(3,4)P2 and PI(3,4,5)P3 lipids (for simplicity termed PI3Ps). As shown in Figure 3A and in Supplemental Movie S4 (Supplemental Data), the initially unpolarized cells became polarized with PH(Akt)-YFP enriched at the leading edge toward the pipette, suggesting that front-to-back gradients in PI3P lipids are also present in chemotactic DCs. Application of LY294002, an inhibitor of PI3K (Vlahos et al., 1994), blocked lamellipod extension, cell migration, and chemotaxis of DCs and fibroblasts (data not shown), suggesting that PI3K signaling is necessary for these processes.

Since a simple gradient amplification model would predict that PI3P levels are uniform when a uniform concentration of chemoattractant is applied to cells, we tested whether DCs exposed to a uniform C5a concentration have a gradient in PH(Akt)-YFP distribution. Since cells can have different relative plasma membrane concentrations at different ends (if they have asymmetric membrane ruffling activities), we used a fluorescent plasma membrane marker as a reference to normalize the PH(Akt)-YFP signals to the local plasma membrane concentration. A suitable marker is a CFP-tagged farnesylated and polybasic peptide that was derived from the K-Ras tail (we also tested a myristoylated and palmitoylated plasma membrane-targeted CFP with a similar result; data not shown). Figure 3B shows examples of dual images (midsection) of unpolarized and polarized DCs expressing the plasma membrane marker and the PH(Akt) domain (z axis serial sections of the cells are shown in Supplemental Figure S3). Using this normalization strategy, we found also in the presence of uniform chemoattractant a several-fold relative enrichment of PH(Akt)-YFP at the actin-rich front of cells (Figures 3C and 3D; confocal sections near the adhesion surface). The observation of a PI3P gradient in the presence of uniform chemoattractant suggests that this gradient is part of the selfpolarization process.

Since the predicted signaling proteins and second messengers in the pathway from chemoattractant receptor to lamellipod extension (G protein, PI3K, PI3P lipids, GEFs, Rac, WASP to Arp2/3; Ridley et al., 2003) are expected to diffuse relatively slowly (diffusion coefficients < 0.5 $\mu m^2/s$; Teruel and Meyer, 2000), it is conceivable that PI3Ps have two roles. They could support front-to-back polarity, but they could also be part of a turn mechanism in which activated receptors at the left or right side of the leading edge selectively induce local PI3P pulses, local lamellipod extensions, and turns to the same side. We therefore investigated whether local PI3P signaling events can be observed within the leading edge of DCs (in uniform C5a) and fibroblasts (in uniform PDGF) by using the dual PH(Akt)-YFP and CFP-CAAX ratio-imaging approach (ratio = PH/CAAX).

Analysis of DCs and fibroblasts showed that both cell types had marked local and transient relative PH(Akt)-YFP increases within the leading edge when the signal was ratioed by the CFP-CAAX signal (Figure 3E). These local pulses were often several-fold above the mean signal in the leading edge (see color calibration) and were not a result of noise since only few local increases were observed in control ratiometric images by using YFP-CAAX and CFP-CAAX membrane probes (Figures 3F and 4A, see Supplemental Movie S5 in the Supplemental Data). Typical sizes of these local PI3P pulses were 3–10 μm^2 (Figure 4B), and typical durations were 30–90 s (Figure 4C). PI3P pulses were triggered stochastically, and separate pulses could be observed along the leading edge several times per minute (Figure 4D; Supplemental Figure S7; Supplemental Movies S6–S8 in the Supplemental Data). The PI3P increase during a pulse can best be explained as a rapid and transient local production, while the decrease is likely a result of both diffusion of PI3Ps away from the site as well as degradation (Figure 4E; Supplemental Figure S6). Similar results were obtained when the PI3P pulses were visualized by total internal reflection fluorescence microscopy (TIRF) at the bottom surface of fibroblasts (Supplemental Figure S4). An earlier measured diffusion coefficient of $\sim$0.5 $\mu m^2/s$ and a lifetime of PI3P lipids of approximately 30–90 s (Haugh et al., 2000) are consistent with the interpretation that diffusion and degradation are terminating a transient local production of PI3P lipid. An upper limit for the PI3P lifetime in DCs was determined by blocking PI3K activity by using LY294002 and Wortmannin and by measuring the rate at which PH domains are released from the membrane (Figure 4F; lifetime < 74 s ± SD = 20 s). This time is faster than the transient PH domain translocation observed in the absence of the addition of the PI3-kinase inhibitors (halftime = 150 s; see Supplemental Figure S5).

An interesting technical observation from these ratio-images was that many sites of local PH(Akt)-YFP enrichment disappeared in the PH/CAAX ratio images and therefore did not reflect a higher relative membrane concentration of PI3Ps. These local enrichments in PH(Akt)-YFP were instead a reflection of ruffles or similar increased local membrane concentrations that are not resolved by light microscopy (Figure 3E). Finally, it is important to point out that our studies were focused on spatial sensing within the leading edge of the cells, where most of these local PI3P pulses were observed and where previous studies found much stronger chemoattractant receptor signaling (Xu et al., 2003; Zigmond et al., 1981).

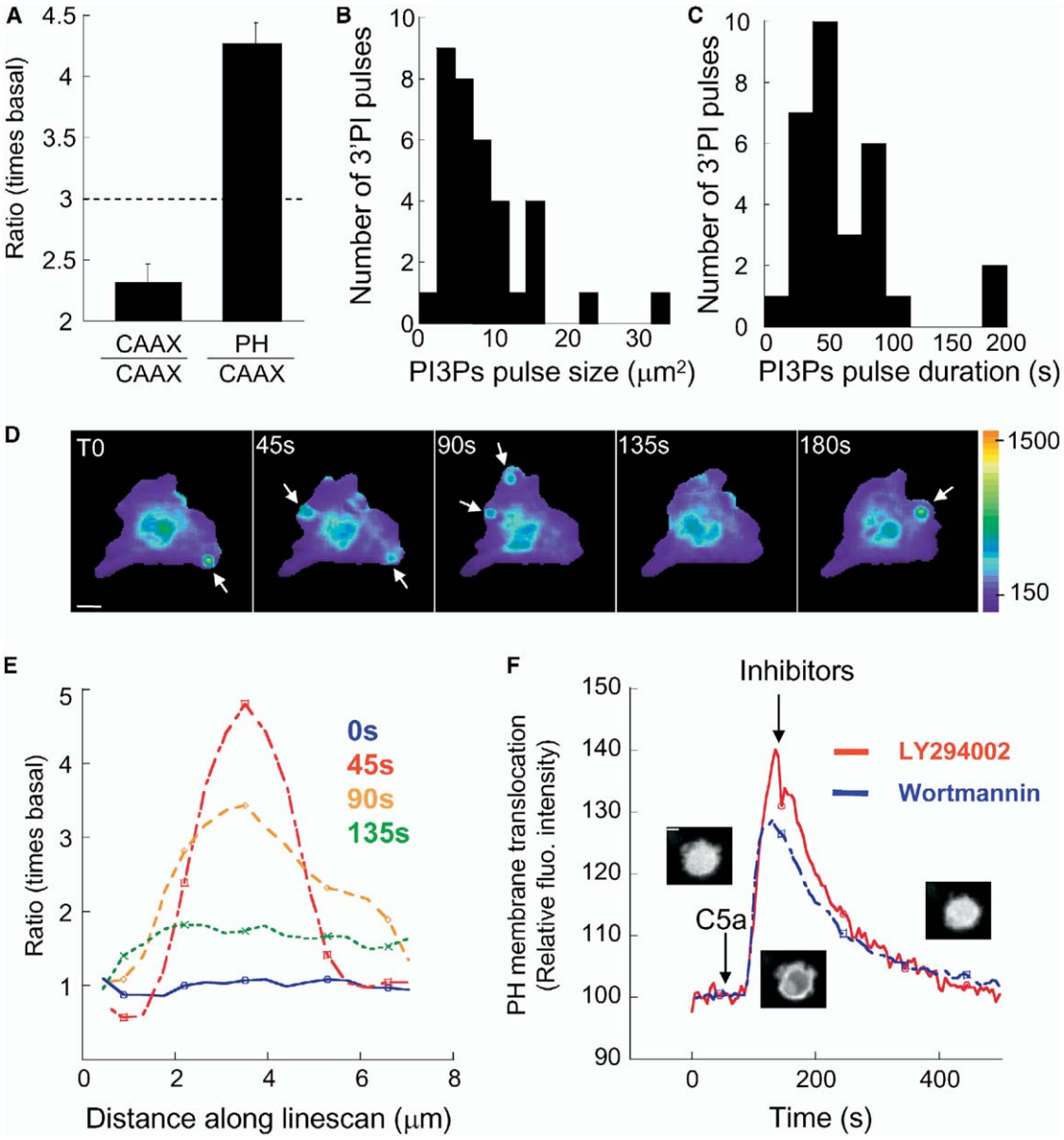

Figure 4. Local and Transient PI3P Pulses Are Triggered Stochastically within the Leading Edge of Migrating DCs

(A) Quantification of local PI3P pulses in DCs. Maximal relative ratio within the leading edge (basal mean ratio was 1; 2 × 2 μm region) compared for PH/CAAX versus a control CAAX/CAAX. A threshold of 3 was chosen for measuring peak areas based on the imaging noise in the CAAX/CAAX control measurements.

(B) Histogram of the size of PI3P pulses. The median size was ~4 μm^2.

(C) Histogram of the duration of individual PI3P pulses. The median duration of the pulses was ~60 s (mean full width at half-maximum).

(D) Sequential images showing stochastic triggering of local PI3P pulses (white arrows) along the leading edge of a DC.

(E) Line-scan analysis of the kinetics of the formation and disappearance of a local PI3P pulse indicates a local production process that is followed by PI3P diffusion and possible degradation. Ratiometric measurements were taken at t = 0 s, 45 s, 90 s, and 135 s in a DC migrating in a uniform C5a concentration (25 nM).

(F) Measurement of an estimated half-life of PI3P lipids by using addition of the PI3K inhibitors LY294002 (50 μm) or Wortmannin (100 nM). The half-life was estimated in C5a pretreated DCs by measuring the translocation of YFP-PH from the membrane back to the cytosol after drug addition. Estimated lifetimes ranged from 30 to 100 s.

Coupling of Local Signaling to Local Lamellipod Extension

We then addressed the question of whether these local PI3P signals correlate with local lamellipod extensions. Given that a few percent more such binding events are expected to occur on the side closer to the source (higher local concentration), one would predict that turns occur more often toward than away from the direction of the source. Indeed, as shown in the images in Figure 5A and Supplemental Figure S8 for fibroblasts, a triggering of local PI3P pulses (PH/CAAX ratio) was often followed by local extensions of lamellipodia (rela-

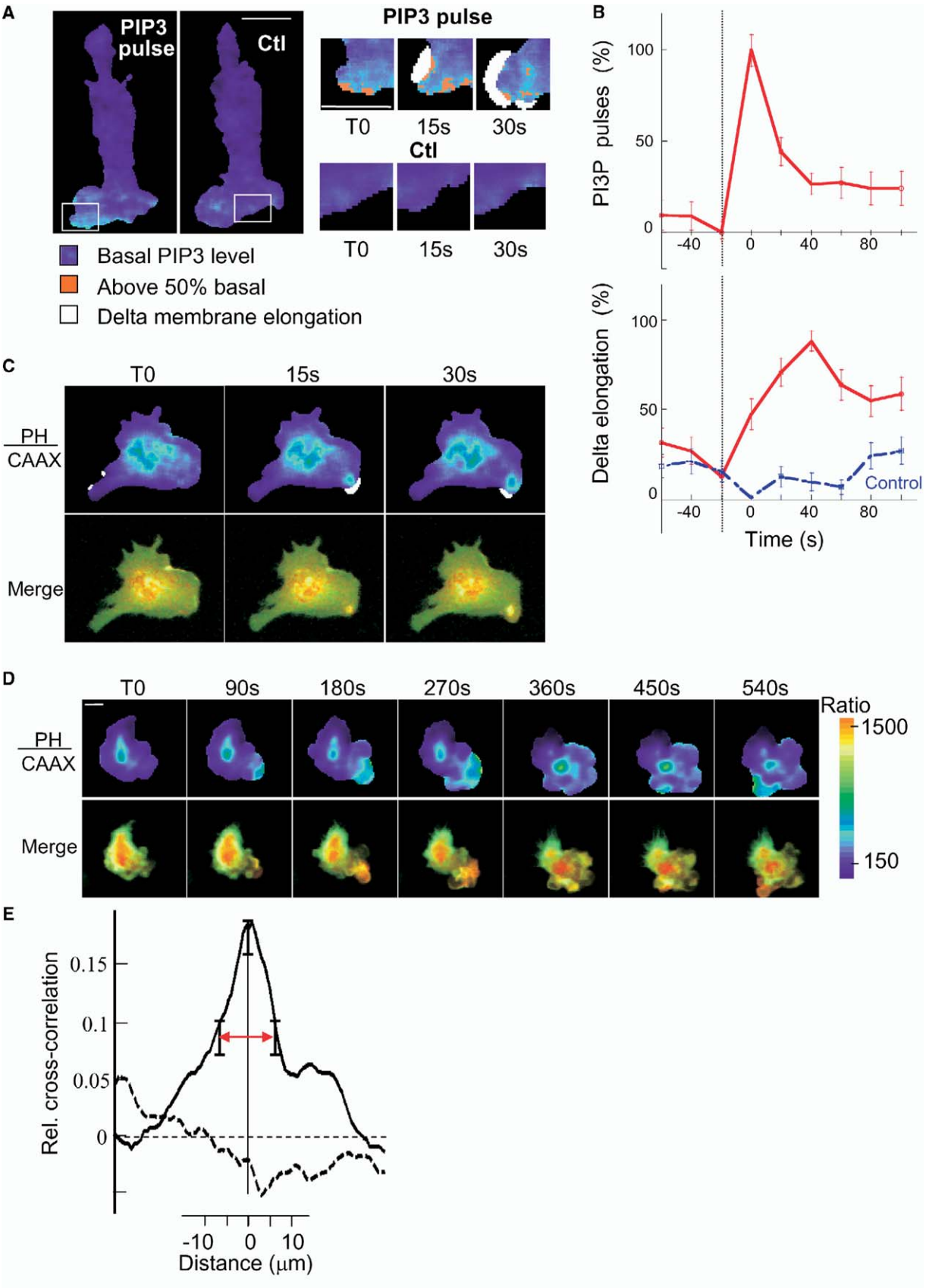

Figure 5. Local PI3P Pulses Correlate with Local Membrane Extensions in Fibroblasts and DCs

(A and B) (A) Quantitative measurement of PI3P pulses and lamellipod extension in a series of images in fibroblasts. PI3P pulses and lamellipod extension were correlated by overlaying ratiometric images (pseudocolored PH/CAAX images) and differential membrane elonga-

tive membrane elongation in white). This was quantified by measuring for each significant increase in the local ratio signal (that went 50% above basal, see the Experimental Procedures) whether a subsequent lamellipod extension occurred near that site (within 5 μm of the PI3P pulse). Figure 5B shows a time course analysis of lamellipod extension at the same site versus a reference site on the opposite end of the leading edge where no local PI3P pulse was observed. For more than 80% of the pulses, they preceded significant lamellipod extension 20–40 s later.

In DCs, the time between local PI3P pulses (in pseudocolor) and lamellipod extensions (in white) was shorter, as is apparent in an example of a series of ratio-images and merged images of a DC in which PH(Akt)-YFP and CAAX-CFP are compared (Figure 5C). A different example of a cell in which PI3P signals are correlated with local membrane extensions that then result in turns in the direction of migration is shown in Figure 5D and in Supplemental Movies S9–S12 (in the Supplemental Data). Since PI3P signals were often followed by membrane extensions in the next frame (15 s later), we performed a crosscorrelation analysis that allows one to measure whether PI3P signals and membrane extension are significantly correlated (Figure 5E). Local membrane extension was measured as the extension distance along the perimeter of a cell, F(x) (in μm; with x as the linearized position along the perimeter; see legend of Figure 2D), and the local PH/CAAX ratio was measured as the ratio R(x) = PH(x)/CAAX(x) with the same position parameter along the perimeter x (in relative units; PH(x) and CAAX(x) were integrated over the outer 2 μm perimeter region; 8 cells and 540 images were used for the analysis). Figure 5E shows the resulting normalized crosscorrelation function, $G(x) = \Sigma F(x_0)^*R(x_0 - x)$. The dashed control correlation line in the same figure was tested for systematic noise by comparing PI3P signals with membrane extensions shifted by 30 μm to the left. Standard errors are shown for three of the data points. Consistent with a local coupling hypothesis, there was a significant correlation between PI3P signals and membrane extension over a distance of ±6.3 μm (full width at half-maximum, red arrow). A correlation of 1 would reflect an extension that is exactly proportional to the PI3P signal. It should be pointed out that while local PI3Ps markedly increased the probability that a local lamellipod extension was triggered, not all observed local PI3P pulses led to lamellipod extension, and only ~70% of all lamellipod extensions were preceded by significant PI3P pulses. This is either a result of the confocal imaging experiments, in which we monitor only a single plane that may only show a fraction of the occurring PI3P signals, or, alternatively, local pulses of PI3Ps that are not the only mediator for triggering local lamellipod extension.

Since PDGF and C5a receptors are both activators of PI3K, and since PI3K activation is known to support the induction of lamellipodia, these local correlation data suggest that PDGF and C5a receptor stimuli can be directly coupled to local membrane extension within the leading edge and thereby trigger small turns in the direction of migration.

Validation of the Local Coupling Model for Eukaryotic Chemotaxis by Computer Simulation

Based on these results, we propose that eukaryotic chemotaxis can best be explained as a local coupling process. In this model, lamellipod extension is a local process that occurs primarily within the leading edge of a polarized cell, and each local lamellipod extension not only triggers a forward movement but also a small turn to the left or right depending on the location of the locally extended lamellipod. The local coupling model then argues that each receptor-chemoattractant interaction within the leading edge creates a local signal that increases the probability that a lamellipod is extended locally (within a few micrometers).

How can such a local coupling lead to correct sensing of a chemoattractant concentration gradient? Assuming that all chemotaxing cells have a capacity for adaptation (Ming et al., 2002), the probability for triggering a local lamellipod extension within the leading edge should be proportional to the relative local chemoattractant concentration. For example, in a cell that migrates perpendicular to the source of the chemoattractant, the probability of triggering a lamellipod to move toward the source is slightly higher than of triggering one to move away from the source (in a shallow gradient 1%–4% higher), which can then turn the cell more often toward than away from the source. The average small turn triggered by an individual local lamellipod extension can be termed "an angular step size," δ. Given the length of fibroblasts and DCs and the dimensions of the observed local lamellipod extensions (Figure 2G), typical angular step sizes are expected to be in the range of 0.5°–4°.

We developed a computer simulation program for this local coupling model by only assuming that a local lamellipod extension within the leading edge is triggered in response to the stochastic local binding of a chemoattractant molecule. The binding probability was proportional to the relative local chemoattractant concentration. Figure 6A (and Supplemental Movie S13 in

tion images (in white). Ratio intensity values that were 50% above basal (control region within leading edge) were colored in red. Control regions (Ctr) and PIP3 pulse regions within the leading edge were chosen for the quantitative analysis in (B) based on their PH/CAAX ratio.
(B) Correlation analysis comparing the triggering of local PI3P pulses (top panel) and the subsequent local extension of a lamellipodia within 5 μm of the site (with a delay of –60, –40, –20, 0, 20, 40, 60, 80, or 100 s; red trace in the bottom panel). A control correlation analysis (blue in bottom panel) that used control regions with low PI3P levels such as the one in (A) is also shown.
(C) Quantitative measurement of PI3P pulses (in pseudocolor) and lamellipod extension (in white) in a series of images in DCs.
(D) Example of a DC in which local PI3P signals correlate with membrane extensions that lead to turns in the direction of migration. All scale bars in the images, 10 μm.
(E) Crosscorrelation analysis showing a significant correlation between local PI3P pulses and local subsequent membrane elongation (correlation distance ~10 μm; n = 500 image pairs).

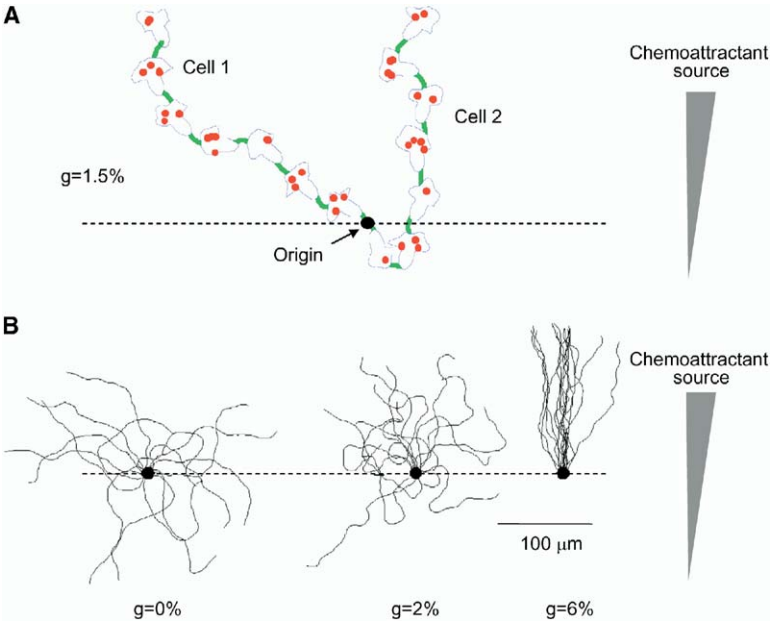

Figure 6. Computer Simulation of Migration Paths with a Local Coupling Model for Chemotaxis

(A) Simulation of random biased walk toward a chemoattractant source when a cell is exposed to a shallow gradient of chemoattractant (g = 1.5%). Two different cells are shown to migrate in the same gradient. Each red dot marks a local receptor stimulus (with a probability to occur assumed to be proportional to the relative local concentration) that then triggers a local lamellipod extension and a small turn in the direction of migration. (B) The migration of 15 cells was simulated in the presence of a uniform chemoattractant (0%, left), the presence of a shallow gradient (2%, middle), and in the presence of a steeper concentration gradient (6%, right).

the Supplemental Data) show that this model is sufficient to make cells migrate more often toward a chemoattractant source than away from it, thereby creating a biased random walk similar to the one observed for fibroblasts, neutrophils, and DCs. Since we were interested in whether such a model could predict a transition from random walk to biased random walk to persistent chemotaxis, we also tested the same simulations for an increasing steepness of the chemoattractant gradient. Strikingly, cells showed a transition from random migration (for uniform chemoattractant and chemoattractant gradients $<\sim 0.5\%$), to biased random walk (0.5%–4%), to persistent migration (>4%). Each of the three panels in Figure 6B shows migration paths of 15 cells that were simulated for gradients of g = 0, g = 0.02, and g = 0.06, respectively. The mean angular step size for the simulation was $\sim 0.7°$.

These simulations show that a local coupling model for eukaryotic chemotaxis predicts the experimentally observed migration paths in uniform chemoattractant concentration as well as in shallow and steep chemoattractant gradients. The observed transition from random migration to chemotaxis is likely physiologically relevant since leukocytes and other cells can then explore the organ space by random migration until they get within the range of target sites, where they can read the chemoattractant gradient. As part of this process, they would undergo a transition from random walk to biased random walk until they could persistently chemotax toward the site of infection or inflammation or other target site. Thus, random migration and chemotaxis provide an effective combined mechanism to increase the capture radius over which cells can be attracted.

Derivation of a General Chemotaxis Equation and Identification of a Compass Parameter

While these simulations are useful for visualizing the cellular migration behavior, we asked the question of whether the directional choices during chemotaxis are directly predictable from basic parameters. It is, for example, apparent from Figure 6 that cells migrate increasingly more often toward the source as the steepness of the gradient increases. These directional choices of migrating cells can be quantitatively described by introducing a directional probability function (or angular probability distribution), $P(\alpha)$ (Figure 7A). The angle α (in units of radian from $+\pi$ to $-\pi$) is the migration angle of a cell in relationship to the chemoattractant source (with an $\alpha = 0$ for a cell migrating toward the source, $+\pi/2$ and $-\pi/2$ for a cell migrating perpendicular to the source, and $-\pi$ for a cell moving away from the source). Based on the assumption that each local signal triggers a small direction change either to the left or right (by an angular step size), we were able to derive a surprisingly simple chemotaxis equation that gives the probability distribution as a function of the gradient steepness, g (fraction of 1, where 1 is a 100% gradient across the leading edge), and the turn angle per signaling event, δ (angular step size in radian).

The chemotaxis equation (Equation 1) is as follows (see the Supplemental Data for derivation):

$$P(\alpha) = \gamma e^{\frac{g}{\delta}\cos(\alpha)}, \qquad (1)$$

where $-\pi < \alpha < \pi$ and γ as a normalization constant.

This chemotaxis equation can be used to describe the directional choices during random migration, biased random walk, and persistent chemotaxis. More importantly, and relevant for the conceptual understanding of chemotaxis, this equation makes the prediction that the different chemotactic migration behaviors of a cell can be described by a single parameter, the ratio CP = g/δ. We have termed this ratio the "compass parameter" since its value is a measure of how well a cell can find the source of a chemoattractant (the higher the value, the better the compass). The compass parameter has a value of CP > 4 for a persistently che-

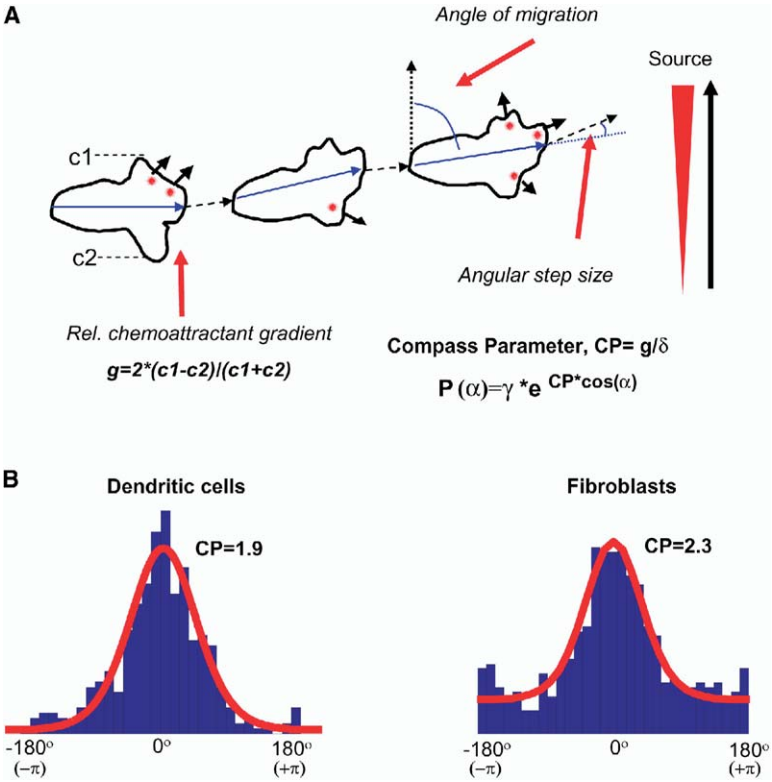

Figure 7. Derivation of a Chemotaxis Equation and Identification of a Compass Parameter

(A) A schematic representation of the local coupling model used to simulate cell migration and chemotaxis. The model predicts that chemotaxis can be described by a single compass parameter that defines a cell's directional choice.

(B) Angular probability chemotaxis plots showing the experimentally measured directional choices during biased random walk as a histogram. The data were fit to the chemotaxis equation to determine the compass parameter, CP = g/δ, for fibroblasts and DCs in a Dunn chamber. The left graph shows data from DCs, and the right graph shows data from fibroblasts. The fit for fibroblasts made an assumption that a fraction of the cells does not participate in the chemotaxis response.

motactic cell, of CP ~0.5–4 for a cell that undergoes biased random walk, and of CP < 0.5 for a randomly migrating cell (see Figure 6B for an illustration of this classification; the respective CPs are 0, 1.65, and 5). One can argue that this parameter is all that one needs to know to predict the overall chemotactic migration paths.

We then determined whether the observed migration directions of DCs and fibroblasts are similar to the ones predicted by this model. When fitting the chemotaxis equation to the experimental directional probability plots (Figure 7B; directional angles were measured by tracking the biased random walk of cells in Figures 1E and 1F), we found a good match with the measured directional probability distribution (CP of 1.9 and 2.3, respectively). This is consistent with estimates for the angular step sizes in the two cell types of 1° and an approximate relative gradient steepness of 3% across the leading edge of the cells. This shows that a quantitative prediction of DC and fibroblast chemotaxis migration paths can be obtained by simply calculating the directional probability by using the chemotaxis equation and the compass parameter.

Conclusions

Our study shows that random migration, biased random walk toward chemoattractants, and persistent chemotaxis can be simulated by a local coupling model and that the fidelity of migrating toward the source can be predicted by a single "compass parameter." The model differs from previous models by arguing that chemotaxis does not involve spatial feedback and that cells do not know where the source of the chemoattractant is at a given moment. Instead, cells only bias stochastic turns more often toward the source than away from it because of a higher receptor binding rate on the side of the leading edge closer to the source.

Most previous chemotaxis models have used long-range "global" cellular feedbacks across the cell that integrate and then amplify the external concentration gradient in order to explain how cells chemotax (spatial integration of receptor signals). While our study is consistent with a role of PI3P signals in selfpolarization (Figure 2 and, for example, Bourne and Weiner, 2002; Postma et al., 2004), we are proposing that this global role of PI3Ps is not related to the chemotaxis process itself. A way to possibly phrase this better is that selfpolarization and a cell's capacity to migrate are fundamental processes needed for a broad range of cell functions and not only for chemotaxis alone (also see, for example, Devreotes and Janetopoulos, 2003). Several previous findings concerning PI3Ps and chemotaxis can then potentially be explained by a dual role of this ubiquitous second messenger in selfpolarization as well as in triggering small turns in the direction of migration. In our model, the only molecular machinery for chemotaxis is the local process by which a local chemoattractant binding event triggers via PI3Ps or other signaling pathways a local lamellipod extension and a small turn in the direction of migration.

Finally, it is interesting to point out that the observed biased random migration paths are, at first glance, reminiscent of the biased random walks seen in bacterial chemotaxis (Sourjik and Berg, 2004). However, the eukaryotic chemotaxis model described here relies on gradual turns that are biased toward the source, while

bacteria reorient their direction randomly after a straight movement phase. Furthermore, the sensing of the concentration gradient can occur in the local coupling model across the front of the cell (spatial sensing), while the much smaller bacteria lacks this ability and uses instead sequential chemoattractant sensing (temporal sensing). This implies that bacteria and eukaryotic cells have developed two different mechanisms to create biased random walks that nevertheless enable both to find the source of chemoattractants.

Experimental Procedures

Preparation of DCs and Transfection

Monocyte-derived DCs were differentiated after a week of culture in the presence of IL-4 (100 ng/ml) and GM-CSF (50 ng/ml) (Preprotech, London, UK). The DCs (2.10^6 cells) were electroporated with 1 μg DNA by using Amaxa's Nucleofector technology (Amaxa biosystem, Koeln, Germany), and experiments were performed between 4 hr and 8 hr after transfection on coverslips coated with fibronectin. NIH3T3 fibroblasts were maintained and transfected as described previously (Haugh et al., 2000).

Chemotaxis Measurements

Chemotaxis and random migration experiments were performed at 37°C in a Dunn chemotaxis chamber (Weber Scientific International, England) by using a stable gradient or uniform concentration of chemoattractant as previously described (Zicha et al., 1991).

Micropipette migration assays were performed by using a micropipette filled with chemoattractant (0.45 μM C5a) to generate gradients based on a C5a point source. C5a was left to passively diffuse out of the pipette. A dextran-rhodamine fluorescent probe (Molecular Probes, Eugene, OR) was used to monitor gradients as a function of time.

Quantification of Membrane Extension

Differential membrane extensions were quantified by subtracting sequential images of cells expressing a membrane marker (CAAX-CFP). A detailed description of the image processing and of the cell-tracking program is provided as Supplemental Data.

PI3P Localization

PI3P localization was investigated in DCs and fibroblasts by monitoring PH(Akt)-YFP translocation as previously described (Kontos et al., 1998). A membrane marker (CAAX-CFP) was used as a reference. Local PI3P enrichment was quantified by ratiometric analysis of the PH probe over the membrane marker (after background subtraction). Ratiometric images of CAAX-YFP and CAAX-CFP were used as controls (see details in the Supplemental Data).

Correlation between PI3P Pulses and Local Membrane Extension

The correlation between PI3P pulses and the induction of lamellipod extension was analyzed by measuring the lamellipod extension by using image subtraction ($T_{m+1} - T_m$) and by measuring PI3P pulses by using PH/CAAC ratiometric images (T_m). Overlays of the subsequent lamellipod extension image and the PI3P ratio image were used to illustrate the correlation between PI3Ps and local membrane extension. For fibroblasts, 34 PI3P pulses were synchronized (set to t = 0), and the relationship to lamellipod extension was analyzed before and after the triggering of the PI3P pulses at the same site (within a 5 μm region) and at a different site outside that region. Using the binary lamellipod data from the $T_{m+1} - Tm$ image stacks, we determined the percent chance that a lamellipod was extended at the same site. Control lamellipod extension was quantified by following membrane elongation at sites without PI3P pulses. For DCs, a crosscorrelation analysis was used (see details in the Supplemental Data).

Supplemental Data

Supplemental Data including a computer simulation, chemotaxis model calculation, derivation of the chemotaxis equation and compass parameter, Experimental Procedures, 8 figures, and 13 movies are available at http://www.developmentalcell.com/cgi/content/full/8/2/215/DC1/.

Acknowledgments

We would like to thank members of the Meyer laboratory for valuable discussions and Drs. Lubert Stryer, Alain Trautmann, and Annette Salmeen for their significant input into the paper. This work was supported by the National Institutes of Health.

Received: October 1, 2004
Revised: October 1, 2004
Accepted: December 9, 2004
Published: February 1, 2005

References

Allen, W.E., Zicha, D., Ridley, A.J., and Jones, G.E. (1998). A role for Cdc42 in macrophage chemotaxis. J. Cell Biol. *141*, 1147–1157.

Bailly, M., Wyckoff, J., Bouzahzah, B., Hammerman, R., Sylvestre, V., Cammer, M., Pestell, R., and Segall, J.E. (2000). Epidermal growth factor receptor distribution during chemotactic responses. Mol. Biol. Cell *11*, 3873–3883.

Bourne, H.R., and Weiner, O. (2002). A chemical compass. Nature *419*, 21.

Condeelis, J., Hall, A., Bresnick, A., Warren, V., Hock, R., Bennett, H., and Ogihara, S. (1988). Actin polymerization and pseudopod extension during amoeboid chemotaxis. Cell Motil. Cytoskeleton *10*, 77–90.

Deuel, T.F., Kawahara, R.S., Mustoe, T.A., and Pierce, A.F. (1991). Growth factors and wound healing: platelet-derived growth factor as a model cytokine. Annu. Rev. Med. *42*, 567–584.

Devreotes, P., and Janetopoulos, C. (2003). Eukaryotic chemotaxis: distinctions between directional sensing and polarization.. J. Biol. Chem. *278*, 20445–20448.

Downey, G.P. (1994). Mechanisms of leukocyte motility and chemotaxis. Curr. Opin. Immunol. *6*, 113–124.

Funamoto, S., Meili, R., Lee, S., Parry, L., and Firtel, R.A. (2002). Spatial and temporal regulation of 3-phosphoinositides by PI 3-kinase and PTEN mediates chemotaxis. Cell *109*, 611–623.

Hannigan, M., Zhan, L., Li, Z., Ai, Y., Wu, D., and Huang, C.K. (2002). Neutrophils lacking phosphoinositide 3-kinase gamma show loss of directionality during N-formyl-Met-Leu-Phe-induced chemotaxis. Proc. Natl. Acad. Sci. USA *99*, 3603–3608.

Haugh, J.M., Codazzi, F., Teruel, M., and Meyer, T. (2000). Spatial sensing in fibroblasts mediated by 3′ phosphoinositides. J. Cell Biol. *151*, 1269–1280.

Iijima, M., and Devreotes, P. (2002). Tumor suppressor PTEN mediates sensing of chemoattractant gradients. Cell *109*, 599–610.

Janetopoulos, C., Ma, L., Devreotes, P.N., and Iglesias, P.A. (2004). Chemoattractant-induced phosphatidylinositol 3,4,5-trisphosphate accumulation is spatially amplified and adapts, independent of the actin cytoskeleton. Proc. Natl. Acad. Sci. USA *101*, 8951–8956.

Kontos, C.D., Stauffer, T.P., Yang, W.P., York, J.D., Huang, L., Blanar, M.A., Meyer, T., and Peters, K.G. (1998). Tyrosine 1101 of Tie2 is the major site of association of p85 and is required for activation of phosphatidylinositol 3-kinase and Akt. Mol. Cell. Biol. *18*, 4131–4140.

Kutscher, B., Devreotes, P., and Iglesias, P.A. (2004). Local excitation, global inhibition mechanism for gradient sensing: an interactive applet. Sci STKE *219*, pl3.

Levchenko, A., and Iglesias, P.A. (2002). Models of eukaryotic gradient sensing: application to chemotaxis of amoebae and neutrophils. Biophys. J. *82*, 50–63.

Lipton, A., Klinger, I., Paul, D., and Holley, R.W. (1971). Migration of mouse 3T3 fibroblasts in response to a serum factor. Proc. Natl. Acad. Sci. USA *68*, 2799–2801.

Meili, R., Ellsworth, C., Lee, S., Reddy, T.B., Ma, H., and Firtel, R.A. (1999). Chemoattractant-mediated transient activation and membrane localization of Akt/PKB is required for efficient chemotaxis to cAMP in *Dictyostelium*. EMBO J. *18*, 2092–2105.

Meinhardt, H. (1999). Orientation of chemotactic cells and growth cones: models and mechanisms. J. Cell Sci. *112*, 2867–2874.

Ming, G.L., Wong, S.T., Henley, J., Yuan, X.B., Song, H.J., Spitzer, N.C., and Poo, M.M. (2002). Adaptation in the chemotactic guidance of nerve growth cones. Nature *417*, 411–418.

Mrowietz, U., Koch, W.A., Zhu, K., Wiedow, O., Bartels, J., Christophers, E., and Schroder, J.M. (2001). Psoriasis scales contain C5a as the predominant chemotaxin for monocyte-derived dendritic cells. Exp. Dermatol. *10*, 238–245.

Niggli, V. (2000). A membrane-permeant ester of phosphatidylinositol 3,4, 5-trisphosphate (PIP(3)) is an activator of human neutrophil migration. FEBS Lett. *473*, 217–221.

Parent, C.A., Blacklock, B.J., Froehlich, W.M., Murphy, D.B., and Devreotes, P.N. (1998). G protein signaling events are activated at the leading edge of chemotactic cells. Cell *95*, 81–91.

Parent, C.A., and Devreotes, P.N. (1999). A cell's sense of direction. Science *284*, 765–770.

Pierce, G.F., Mustoe, T.A., Lingelbach, J., Masakowski, V.R., Griffin, G.L., Senior, R.M., and Deuel, T.F. (1989). Platelet-derived growth factor and transforming growth factor-beta enhance tissue repair activities by unique mechanisms. J. Cell Biol. *109*, 429–440.

Pollard, T.D., and Borisy, G.G. (2003). Cellular motility driven by assembly and disassembly of actin filaments. Cell *112*, 453–465.

Postma, M., Bosgraaf, L., Loovers, H.M., and Van Haastert, P.J. (2004). Chemotaxis: signalling modules join hands at front and tail. EMBO Rep. *5*, 35–40.

Ridley, A.J., Schwartz, M.A., Burridge, K., Firtel, R.A., Ginsberg, M.H., Borisy, G., Parsons, J.T., and Horwitz, A.R. (2003). Cell migration: integrating signals form front to back. Science *302*, 1704–1709.

Schmidt, A., and Hall, M.N. (1998). Signaling to the actin cytoskeleton. Annu. Rev. Cell Dev. Biol. *14*, 305–338.

Schrick, K., Garvik, B., and Hartwell, L.H. (1997). Mating in *Saccharomyces cerevisiae*: the role of the pheromone signal transduction pathway in the chemotropic response to pheromone. Genetics *147*, 19–32.

Servant, G., Weiner, O.D., Herzmark, P., Balla, T., Sedat, J.W., and Bourne, H.R. (2000). Polarization of chemoattractant receptor signaling during neutrophil chemotaxis. Science *287*, 1037–1040.

Servant, G., Weiner, O.D., Neptune, E.R., Sedat, J.W., and Bourne, H.R. (1999). Dynamics of a chemoattractant receptor in living neutrophils during chemotaxis. Mol. Biol. Cell *10*, 1163–1178.

Sourjik, V., and Berg, H.C. (2004). Functional interactions between receptors in bacterial chemotaxis. Nature *428*, 437–441.

Sozzani, S., Sallusto, F., Luini, W., Zhou, D., Piemonti, L., Allavena, P., Van Damme, J., Valitutti, S., Lanzavecchia, A., and Mantovani, A. (1995). Migration of dendritic cells in response to formyl peptides, C5a, and a distinct set of chemokines. J. Immunol. *155*, 3292–3295.

Tengholm, A., and Meyer, T. (2002). A PI3-kinase signaling code for insulin-triggered insertion of glucose transporters into the plasma membrane. Curr. Biol. *12*, 1871–1876.

Teruel, M.N., and Meyer, T. (2000). Translocation and reversible localization of signaling proteins: a dynamic future for signal transduction. Cell *103*, 181–184.

Tranquillo, R.T., Lauffenburger, D.A., and Zigmond, S.H. (1988). A stochastic model for leukocyte random motility and chemotaxis based on receptor binding fluctuations. J. Cell Biol. *106*, 303–309.

Vlahos, C.J., Matter, W.F., Hui, K.Y., and Brown, R.F. (1994). A specific inhibitor of phosphatidylinositol 3-kinase, 2-(4-morpholinyl)-8-phenyl-4H–1-benzopyran-4-one (LY294002). J. Biol. Chem. *269*, 5241–5248.

Wang, F., Herzmark, P., Weiner, O.D., Srinivasan, S., Servant, G., and Bourne, H.R. (2002). Lipid products of PI(3)Ks maintain persistent cell polarity and directed motility in neutrophils. Nat. Cell Biol. *4*, 513–518.

Xu, J., Wang, F., Van Keymeulen, A., Herzmark, P., Straight, A., Kelly, K., Takuwa, Y., Sugimoto, N., Mitchison, T., and Bourne, H.R. (2003). Divergent signals and cytoskeletal assemblies regulate self-organizing polarity in neutrophils. Cell *114*, 201–214.

Zicha, D., Dunn, G., and Jones, G. (1997). Analyzing chemotaxis using the Dunn direct-viewing chamber. Methods Mol. Biol. *75*, 449–457.

Zicha, D., Dunn, G.A., and Brown, A.F. (1991). A new direct-viewing chemotaxis chamber. J. Cell Sci. *99*, 769–775.

Zigmond, S.H., Levitsky, H.I., and Kreel, B.J. (1981). Cell polarity: an examination of its behavioral expression and its consequences for polymorphonuclear leukocyte chemotaxis. J. Cell Biol. *89*, 585–592.